

# The effect of capping layers on the near-surface region of SrVO<sub>3</sub> films

Shaked Caspi<sup>1</sup>, Lishai Shoham<sup>1</sup>, Maria Baskin<sup>1</sup>, Kamira Weinfeld<sup>2</sup>, Cinthia Piamonteze<sup>3</sup>, Kelsey A. Stoerzinger<sup>4,5</sup>, and Lior Kornblum<sup>1,a)</sup>

<sup>1</sup>Andrew & Erna Viterbi Department of Electrical & Computer Engineering, Technion—Israel Institute of Technology, Haifa 32000-03, Israel

<sup>2</sup>Solid State Institute, Technion—Israel Institute of Technology, Haifa 32000-03, Israel

<sup>3</sup>Swiss Light Source, Paul Scherrer Institute, 5232 Villigen PSI, Switzerland

<sup>4</sup>School of Chemical, Biological and Environmental Engineering, Oregon State University, Corvallis, OR 97331, United States of America

<sup>5</sup>Physical Sciences Division, Pacific Northwest National Laboratory, Richland, WA 99254, United States of America

a) Electronic mail: liork@ee.technion.ac.il

Surfaces of correlated-electron oxides are of significant interest both from fundamental and applied perspectives. Many such oxides feature a near-surface region (NSR) which differs from the bulk's properties. The NSR can significantly affect the interpretation of the material's electronic structure, especially for those in thin film form, and have detrimental effects for applications such as field effect devices and catalysts. In this work we study the changes in the composition and electronic structure of the NSR of SrVO<sub>3</sub> (SVO) thin films. We employ x-ray photoelectron spectroscopy (XPS) and compare TiO<sub>x</sub>-capped SVO films to identical uncapped films that were exposed to ambient conditions. The significant over-oxidation of the SVO surface in the bare film, illustrated by a primary V<sup>5+</sup> component, is prevented by the TiO<sub>x</sub> layer in the capped film. The capped film further exhibits a decrease in Sr surface phases. These results demonstrate the importance and potential of such capping layers in preserving the bulk properties of correlated oxides in their NSR, enabling more accurate probes for their underlying physics and offering a route for their integration into devices.

## I. INTRODUCTION

Materials with electron correlation have attracted considerable scientific attention for nearly a century, owing to their fascinating, sometimes unexpected physics. Advancement in thin film synthesis techniques have heralded prospects of emergent interface physics<sup>1</sup> and of maturing some of these phenomena towards practical devices.<sup>2,3</sup> Moreover, driving thin films into the ultrathin (few nanometers) regime can give rise to interesting electronic and magnetic phenomena, driven by quantum confinement<sup>4-8</sup> and dimensional crossover.<sup>9-12</sup> From a device point of view, the application of an electric field is a desirable strategy for controlling and switching material properties, such as metal-insulator transitions.<sup>2,13-15</sup> Given the typically high carrier densities in such materials,<sup>16</sup> ultrathin films would be required to produce a non-negligible modulation under realistic electric fields.

A common feature of correlated electron materials is that their electronically active cation, e.g., the transition metal in the B-site of perovskite oxides, often has several metastable oxidation states. Furthermore, in many of these materials, the B cation is not in its most stable oxidation state (e.g., Mn<sup>3+</sup> in LaMnO<sub>3</sub>). As a result, when exposed to atmospheric conditions, ions near the surface can be readily tempted by the abundance of oxygen and humidity to chemically react with atmospheric molecules and achieve an oxidation state closer to equilibrium. This results in a near-surface region (NSR) on the films that differs from the bulk in its chemical, structural and electronic properties.<sup>5,17,18</sup> These differences between bulk and surface can be further compounded by the phenomenon of A-site cation enrichment toward the surface of the film.<sup>19-21</sup>

When considering ultrathin films, the NSR might constitute most, or even all of the film volume, prohibiting access to the correlated electron physics of interest.

In this work we chose SrVO<sub>3</sub> (SVO) as a model correlated system. It is a 3d<sup>1</sup> correlated metal,<sup>22</sup> an endmember of a filling-controlled metal-insulator transition system<sup>23</sup> and an attractive earth-abundant transparent conductive oxide,<sup>24</sup> a critical component of solar and optoelectronic devices.

We examine the surface of SrVO<sub>3</sub> and the effect of an ultrathin TiO<sub>x</sub> cap on the NSR. Motivated by a successful implementation of similar caps by Zou et al.<sup>25</sup> for

protecting LaTiO<sub>3</sub> films, we set out to examine the interface of such a capping layer with a correlated material and its effects on the film's NSR.

## II. EXPERIMENTAL

A bare SVO sample and a TiO<sub>x</sub>-capped SVO sample were epitaxially grown in a customized Veeco GenXplor oxide molecular beam epitaxy (MBE) instrument, operated at a base pressure of  $\sim 5 \times 10^{-10}$  Torr. Growth was done on (001) (LaAlO<sub>3</sub>)<sub>0.3</sub>(Sr<sub>2</sub>AlTaO<sub>3</sub>)<sub>0.7</sub> (LSAT) 5×5 mm<sup>2</sup> substrates (CrysTec GmbH). The growth was done at oxygen backpressure of  $\sim 5 \times 10^{-7}$  Torr controlled by a manual leak valve, at 1000°C,<sup>26</sup> as measured by a thermocouple in proximity to a Mo backplate in contact with the sample. The thickness of the SVO films is estimated from the finite thickness oscillations [Fig. 1(a)] to be  $\sim 28.5 \pm 1$  nm. SVO growth was done by a shuttered method<sup>27,28</sup> where a monolayer of Sr and a monolayer of V are alternately deposited onto the surface with the oxygen being kept continuously steady throughout the growth. Sr and V are evaporated from Veeco SUMO and high-temperature sources, respectively. Their atomic fluxes are independently calibrated in vacuum before each growth using a quartz crystal microbalance (QCM). Fine tuning is further done via the shutter times controlled by the growth software. The samples are cooled to room temperature under the same oxygen pressure as the growth.

*In-situ* deposition of the TiO<sub>x</sub> capping layer on the SVO film was performed at an oxygen backpressure of  $8 \times 10^{-7}$  Torr by evaporating Ti from a high-temperature source. Deposition is done during the cooldown of the sample from its growth temperature, starting at 200°C. The nominal thickness of the cap is  $\sim 4$  nm, which was calibrated by x-ray reflectivity (XRR) analysis of a similar layer deposited on a SrTiO<sub>3</sub> substrate (without epitaxial layers). The TiO<sub>x</sub> layer is most likely amorphous, as inferred by the absence of crystalline reflection high energy electron diffraction (RHEED) patterns from its surface and the absence of Bragg reflections in a grazing incidence x-ray diffraction<sup>39</sup> [excluding (102)<sub>SrTiO<sub>3</sub></sub> from the substrate which is near the Bragg condition in this geometry].

Structural characterization was done with high-resolution x-ray diffraction (XRD) using a Rigaku SmartLab with a 2-bounce incident monochromator. The surface

morphology was imaged with an Asylum Research/Oxford Instruments Cypher ES Environmental atomic force microscope (AFM) operated in tapping mode.

X-ray photoelectron spectroscopy (XPS) was used for chemical analysis<sup>29,30</sup> of the SVO surface with and without TiO<sub>x</sub> capping layer. High resolution measurements were acquired with a PHI Versaprobe III using a monochromated x-ray source of Al K $\alpha$  (1486.6 eV). The photoelectrons were collected at a take-off angle of 45° and a pass energy of 55 eV with energy steps of 0.05 eV. The binding energies (BE) were aligned according to the C1s peak (285.0 eV), and curve fitting was done using the CasaXPS software with a Shirley background and a 30% Lorentzian-Gaussian ratio line shape.<sup>31,32</sup>

### III. RESULTS AND DISCUSSION

Structural analysis of the films by XRD [Fig. 1(a)] confirms the high quality of the epitaxial layer for both capped SVO and bare SVO samples, as indicated by the sharp and intense SVO peaks and the abundance of finite thickness oscillations. The out-of-plane lattice parameters of the bare and capped SVO (3.819 Å and 3.830 Å respectively) are in agreement with previous reports, further attesting to their high structural quality<sup>26,33,34</sup>; the small difference between the values is ascribed to small stoichiometry fluctuations between growths.<sup>26</sup>

The topography of the bare and capped films is analyzed by AFM [Fig. 1(b), 1(c), respectively]. The films exhibit smooth surfaces with root mean square (RMS) roughness of ~0.3 nm for the bare SVO sample and ~0.4 nm for the capped sample. The few surface precipitates (~1-2 nm in height, <1 precipitate· $\mu\text{m}^{-2}$ ) that are visible in both films are ascribed to the segregation of Sr-rich phases near the surface, as discussed later within the XPS results.

This is the author's peer reviewed, accepted manuscript. However, the online version of record will be different from this version once it has been copyedited and typeset.  
PLEASE CITE THIS ARTICLE AS DOI: 10.1116/6.0001419

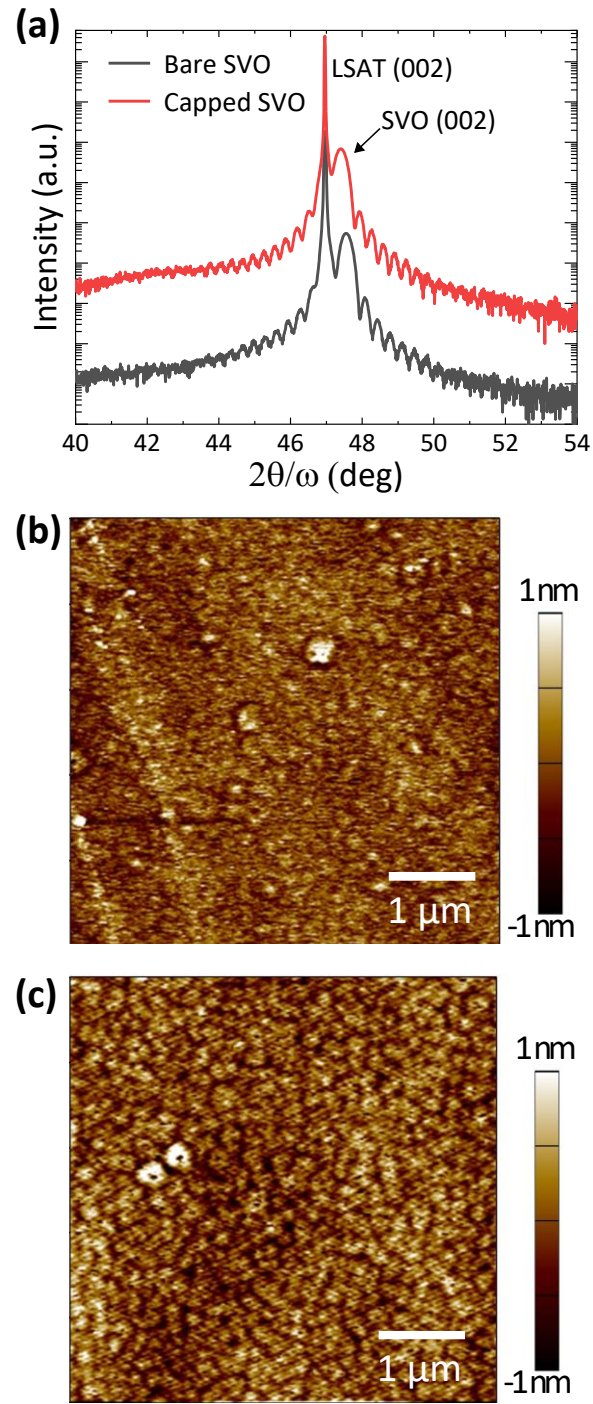


FIG. 1. (a) X-ray diffraction patterns around the (002) Bragg reflection of bare (black) and capped (red) SVO films, grown on LSAT substrates. Representative AFM image of (b) bare and (c) capped SVO films, acquired from an area of  $5 \times 5 \mu\text{m}^2$ .

The chemistry of the  $\text{TiO}_x$  cap layer was inferred from the XPS spectrum of the Ti 2p core level. Most of the Ti 2p<sub>3/2</sub> signal (Fig. 2) is fitted with a  $\text{Ti}^{4+}$  component, accompanied by a small contribution at lower binding energy typical of a  $\text{Ti}^{3+}$  state,<sup>35</sup> constituting 4% of the Ti 2p total area. This indicates that the cap consists of  $\text{TiO}_{2-\delta}$ , namely, it is close to titanium dioxide.

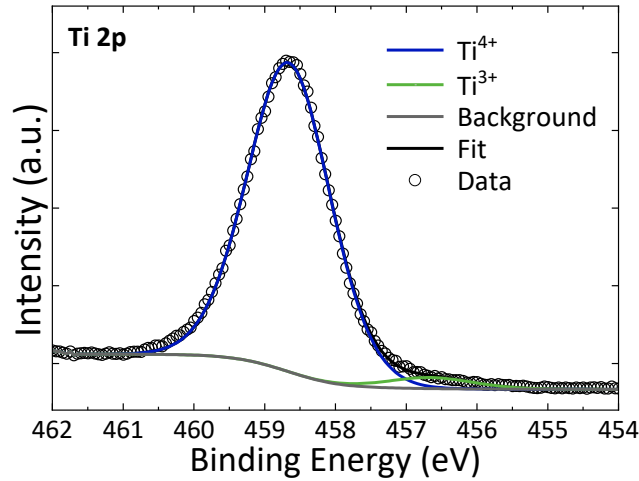


FIG. 2. High resolution XPS spectrum of Ti 2p<sub>3/2</sub> core level of the capped SVO sample.

We now focus on XPS analysis of the SVO surface and how it is affected by the capping layer. Figure 3(a) presents the XPS spectra of O 1s and V 2p core levels of the bare and the capped SVO samples. Since the O 1s signal appears in close proximity to the V 2p doublet, they were all fitted with a single Shirley background.

This is the author's peer reviewed, accepted manuscript. However, the online version of record will be different from this version once it has been copyedited and typeset.  
PLEASE CITE THIS ARTICLE AS DOI: 10.1116/6.0001419

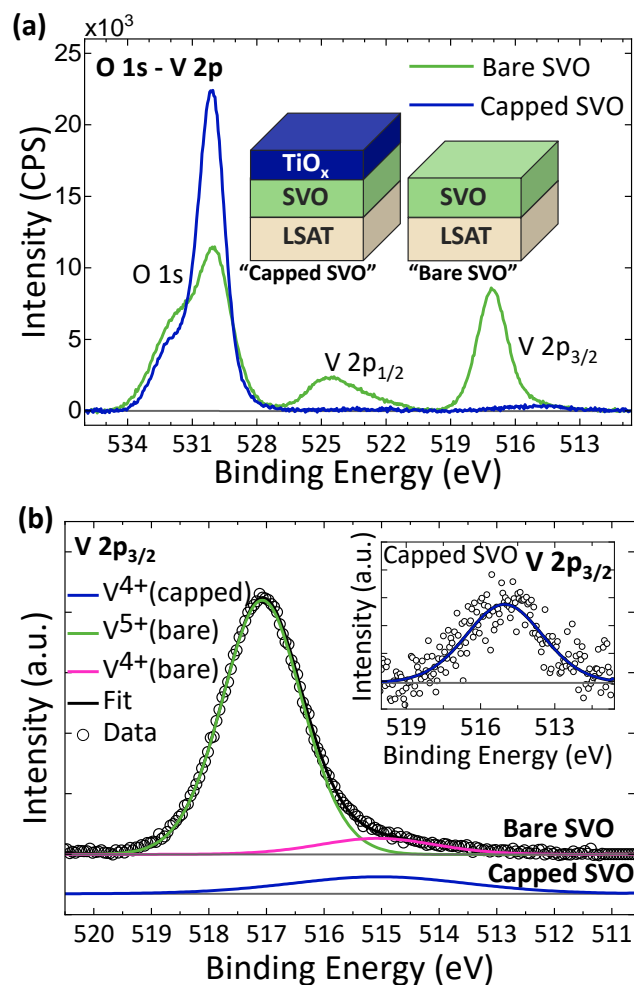


FIG. 3. (a) Background-subtracted XPS spectra of O 1s and V 2p core levels of bare SVO and capped SVO. The inset shows schematic structures of both samples. (b) Fit of the V 2p<sub>3/2</sub> spectral region of bare SVO and capped SVO (inset). The fitted curve of the capped SVO is also presented, magnified and vertically shifted, under the bare SVO signal, for comparison.

Figure 3(b) focuses on the fit of the V 2p<sub>3/2</sub> spectral region for both the bare and the capped samples. The V 2p<sub>3/2</sub> signal of the bare SVO sample consists of a main component associated with a 5+ oxidation state,<sup>34,36,37</sup> while the remaining low-energy tail can be fitted with a peak related to the V<sup>4+</sup> component of SVO.<sup>37,38</sup> This key observation of this work highlights the tendency of the SVO surface to get over-oxidized when exposed to ambient air, which results from the higher stability of the 5+ state, versus the lower

oxidation states of V. While some surface over-oxidation is to be expected, the dominance of  $V^{5+}$  (>90% of the signal, Table I) in the near-surface region of SVO is noteworthy. We estimate the signal depth to be  $3\sin(\theta)\lambda \approx 4$  nm, where  $\theta$  is the takeoff angle ( $45^\circ$ ) and  $\lambda$  is the inelastic mean free path (IMFP) of the  $V^{5+}$  photoelectrons ( $\sim 1.84$  nm), estimated<sup>39</sup> for stoichiometric SVO according to the TPP-2M equation<sup>40</sup>. The overoxidized NSR in SVO is therefore estimated to be on the order of 10 unit cells.

For the capped sample, the V  $2p_{3/2}$  signal is relatively weak since the SVO film is attenuated by the  $\sim 4$  nm capping layer. This signal is fitted with a single peak [inset of Fig. 3(b)], and it is positioned approximately at the same binding energy as the  $V^{4+}$  component of the bare sample (Table I). This comparison is visually illustrated by a magnified depiction of the fitted curve below the signal of the bare SVO in the main panel of Fig. 3(b).

We note that the fitted  $V^{4+}$  peak is relatively wide for the bare sample (FWHM=3.65 eV), and we raise the possibility that titanium in the cap layer reduces the SVO surface during  $TiO_x$  deposition, similar to the effect observed on  $SrTiO_3$  surfaces.<sup>41</sup> In that case the V  $2p_{3/2}$  signal could be fitted with a slightly narrower  $V^{4+}$  component and a smaller  $V^{3+}$  peak at a lower binding energy.<sup>38</sup> Such a potential scenario is presented in the Supplementary Material<sup>39</sup>. Alternatively, the broad  $V^{4+}$  component could be the result of many-body effects, where the interactions of valence electrons with the core hole, created after the emission of a photoelectron, can result in different final states of the ion, giving rise to the formation of multiple spectral features around the primary peak.<sup>42</sup> Lin et al. discussed these phenomena in various open-shell transition-metal oxides, including  $SrVO_3$ .<sup>37</sup> Other works have shown that screening by the (conducting) electrons near the Fermi level can cause such broadening of the V  $2p$  features.<sup>43,44</sup> At this point we consider all the above as valid explanations for the broad  $V^{4+}$  feature. As such, some surface reduction cannot be fully ruled out at this point, which requires further study and possibly optimization of the cap deposition. Nonetheless, our key observation remains the disappearance of the  $V^{5+}$  component, demonstrating the efficacy of the capping layer in eliminating the over-oxidation of NSR and retaining a predominately  $V^{4+}$  SVO surface.



In the Sr 3d spectral region (Fig. 4), the signal for both the bare and the capped samples is fitted with two doublets. The first doublet, positioned at a lower binding energy, is ascribed to the perovskite structure of the SVO film,<sup>38,45</sup> whereas a broader doublet is positioned at  $1.30 \pm 0.05$  eV higher energy in both samples. This broader component is attributed to other chemical states of Sr which can form as a result of Sr excess near the surface of the film. Such Sr-enrichment has been observed in many perovskite oxides,<sup>46</sup> and can result from segregation of Sr-rich phases to the surface; these could be SrO precipitates, as was shown for example in strontium titanate-based perovskites<sup>47-50</sup> and in SVO.<sup>38</sup> In other cases, the formation of surface Sr-rich Ruddlesden-Popper (RP) phases<sup>51</sup> has been reported in different perovskite oxides<sup>19,52</sup> as well as in SVO films, where structures of  $\text{Sr}_3\text{V}_2\text{O}_8$ <sup>53,54</sup> were identified. Additional surface phases, like  $\text{Sr}(\text{OH})_2$  and  $\text{SrCO}_3$ , have been reported following interaction with ambient air.<sup>49,55-57</sup>

In the Sr 3d spectrum of the bare SVO sample, most of the signal is fitted with the broader surface-related component, while only a small fraction (~5% of the signal) is related to the SVO structure; this is comparable to the fraction of the  $\text{V}^{4+}$  component in the V 2p spectrum of the bare sample (Table I). The capped sample, however, exhibits a significant increase in the area fraction of the SVO component, which corresponds to the decrease of surface Sr phase that attenuates the SVO signal from the bulk.

Comparison of these results with the effect of the caps on the V 2p features allows another conclusion to be drawn: while the cap seems to eliminate the non-SVO V 2p moieties, in the Sr 3d spectrum (Table I), the non-SVO components remain significant (55% of the signal). This observation might indicate that the surface phase of the capped sample is likely SrO, that forms as a result of Sr-enrichment in the NSR. The formation of  $\text{SrCO}_3$  phase on the surface, as a result of a reaction between SrO and  $\text{CO}_2$  from the ambient air,<sup>56</sup> needs to be considered as well, since the C 1s spectra<sup>39</sup> exhibits a small carbonate peak. However, this peak is found in the spectra of both the bare and the capped samples, and because the SVO film in the capped sample was not exposed to ambient air, it is more likely that the carbonate component is originated from adventitious carbon contamination.

These results further support the conclusion that a thin  $\text{TiO}_x$  capping layer, grown *in-situ* on top of the SVO film before exposure to ambient air, can efficiently prevent the formation of surface phases and undesirable chemical states.

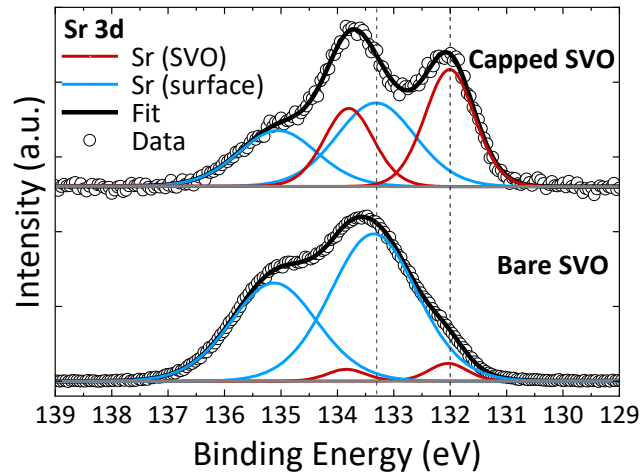


FIG. 4. Background-subtracted XPS spectra and fit of Sr 3d core level for bare SVO (bottom) and capped SVO (top, magnified and vertically shifted for clarity).

#### IV. SUMMARY AND CONCLUSIONS

The chemical states of the near-surface region of SVO films, with and without a protective capping layer, are studied using *ex-situ* XPS analysis. It is demonstrated that a few nanometers thick  $\text{TiO}_x$  cap, which protect the SVO film from exposure to ambient air, can efficiently prevent the over-oxidation of the transition-metal cation and diminish Sr-rich surface phases. A possible reduction of the surface by the cap is not entirely ruled out and could benefit from *in-situ* XPS analysis. Effective capping of correlated oxides provides a better-defined testbed for their physics, which becomes critical the thinner the oxide is. Implementing such caps enables to study ultrathin oxide films and decouple the effect of the near-surface region from their intrinsic physics, an important aspect for future devices.

## ACKNOWLEDGMENTS

We dedicate this work to Scott Chambers, whose decades of leadership in development of this field have made this work possible. Happy birthday!

The authors are grateful to Dr. Maria Koifman Khristosov for her continuous support with XRD characterization and to Dr. Jesús Lacasa for support with AFM measurements. This work was made possible with the support of the Israeli Science Foundation (ISF Grant 375/17), with partial support from the Russell Berrie Nanotechnology Institute (RBNI).

## DATA AVAILABILITY

The entire raw data used to plot the figures of this work is available in an annotated xlsx file, available in the supplementary material.

## REFERENCES

- <sup>1</sup>H.Y. Hwang, Y. Iwasa, M. Kawasaki, B. Keimer, N. Nagaosa, and Y. Tokura, *Nat. Mater.* **11**, 103 (2012).
- <sup>2</sup>Y. Zhou and S. Ramanathan, *Crit. Rev. Solid State Mater. Sci.* **38**, 286 (2013).
- <sup>3</sup>L. Kornblum, *Adv. Mater. Interfaces* **6**, 1900480 (2019).
- <sup>4</sup>M. Choi, C. Lin, M. Butcher, C. Rodriguez, Q. He, A.B. Posadas, A.Y. Borisevich, S. Zollner, and A.A. Demkov, *Appl. Phys. Lett.* **106**, 192902 (2015).
- <sup>5</sup>Y. Hotta, H. Wadati, A. Fujimori, T. Susaki, and H.Y. Hwang, *Appl. Phys. Lett.* **89**, 251916 (2006).
- <sup>6</sup>R.F. Need, P.B. Marshall, E. Kenney, A. Suter, T. Prokscha, Z. Salman, B.J. Kirby, S. Stemmer, M.J. Graf, and S.D. Wilson, *Npj Quantum Mater.* **3**, 7 (2018).
- <sup>7</sup>C.A. Jackson, J.Y. Zhang, C.R. Freeze, and S. Stemmer, *Nat. Commun.* **5**, 4258 (2014).

- <sup>8</sup>J.E. Ortmann, N. Nookala, Q. He, L. Gao, C. Lin, A.B. Posadas, A.Y. Borisevich, M.A. Belkin, and A.A. Demkov, *ACS Nano* **12**, 7682 (2018).
- <sup>9</sup>K. Yoshimatsu, T. Okabe, H. Kumigashira, S. Okamoto, S. Aizaki, A. Fujimori, and M. Oshima, *Phys. Rev. Lett.* **104**, 147601 (2010).
- <sup>10</sup>A. Fouchet, M. Allain, B. Bérini, E. Popova, P.-E. Janolin, N. Guiblin, E. Chikoidze, J. Scola, D. Hrabovsky, Y. Dumont, and N. Keller, *Mater. Sci. Eng. B* **212**, 7 (2016).
- <sup>11</sup>M. Gu, S.A. Wolf, and J. Lu, *Adv. Mater. Interfaces* **1**, 1300126 (2014).
- <sup>12</sup>M. Pickem, J. Kaufmann, K. Held, and J.M. Tomczak, *Phys. Rev. B* **104**, 024307 (2021).
- <sup>13</sup>M. Imada, A. Fujimori, and Y. Tokura, *Rev. Mod. Phys.* **70**, 1039 (1998).
- <sup>14</sup>I.H. Inoue and M.J. Rozenberg, *Adv. Funct. Mater.* **18**, 2289 (2008).
- <sup>15</sup>J. Son, S. Rajan, S. Stemmer, and S. James Allen, *J. Appl. Phys.* **110**, 084503 (2011).
- <sup>16</sup>C. Leighton, *Nat. Mater.* **18**, 13 (2019).
- <sup>17</sup>A. Fouchet, J.E. Rault, M. Allain, B. Bérini, J.-P. Rueff, Y. Dumont, and N. Keller, *J. Appl. Phys.* **123**, 055302 (2018).
- <sup>18</sup>K. Maiti, D.D. Sarma, M.J. Rozenberg, I.H. Inoue, H. Makino, O. Goto, M. Pedio, and R. Cimino, *Europhys. Lett.* **55**, 246 (2001).
- <sup>19</sup>H. Dulli, P.A. Dowben, S.-H. Liou, and E.W. Plummer, *Phys. Rev. B* **62**, R14629 (2000).
- <sup>20</sup>J. Druce, H. Téllez, M. Burriel, M.D. Sharp, L.J. Fawcett, S.N. Cook, D.S. McPhail, T. Ishihara, H.H. Brongersma, and J.A. Kilner, *Energy Environ. Sci.* **7**, 3593 (2014).
- <sup>21</sup>M. Choi, I.A.M. Ibrahim, K. Kim, J.Y. Koo, S.J. Kim, J.-W. Son, J.W. Han, and W. Lee, *ACS Appl. Mater. Interfaces* **12**, 21494 (2020).
- <sup>22</sup>J.A. Moyer, C. Eaton, and R. Engel-Herbert, *Adv. Mater.* **25**, 3578 (2013).
- <sup>23</sup>S. Miyasaka, T. Okuda, and Y. Tokura, *Phys. Rev. Lett.* **85**, 5388 (2000).

- <sup>24</sup>L. Zhang, Y. Zhou, L. Guo, W. Zhao, A. Barnes, H.-T. Zhang, C. Eaton, Y. Zheng, M. Brahlek, H.F. Haneef, N.J. Podraza, M.H.W. Chan, V. Gopalan, K.M. Rabe, and R. Engel-Herbert, *Nat. Mater.* **15**, 204 (2016).
- <sup>25</sup>K. Zou, S. Ismail-Beigi, K. Kisslinger, X. Shen, D. Su, F.J. Walker, and C.H. Ahn, *APL Mater.* **3**, 036104 (2015).
- <sup>26</sup>L. Shoham, M. Baskin, M.-G. Han, Y. Zhu, and L. Kornblum, *Adv. Electron. Mater.* **6**, 1900584 (2020).
- <sup>27</sup>J.H. Haeni, C.D. Theis, and D.G. Schlom, *J. Electroceramics* **4**, 385 (2000).
- <sup>28</sup>Y.F. Nie, Y. Zhu, C.-H. Lee, L.F. Kourkoutis, J.A. Mundy, J. Junquera, P. Ghosez, D.J. Baek, S. Sung, X.X. Xi, K.M. Shen, D.A. Muller, and D.G. Schlom, *Nat. Commun.* **5**, 4530 (2014).
- <sup>29</sup>S.A. Chambers, in *Hard X-Ray Photoelectron Spectrosc.*, edited by J. Woicik (Springer International Publishing, Cham, 2016), pp. 341–380.
- <sup>30</sup>O.Q. Carvalho, E.J. Crumlin, and K.A. Stoerzinger, *J. Vac. Sci. Technol. A* **39**, 040802 (2021).
- <sup>31</sup>G.H. Major, N. Fairley, P.M.A. Sherwood, M.R. Linford, J. Terry, V. Fernandez, and K. Artyushkova, *J. Vac. Sci. Technol. A* **38**, 061203 (2020).
- <sup>32</sup>D. Cohen-Azarzar, M. Baskin, and L. Kornblum, *J. Appl. Phys.* **123**, 245307 (2018).
- <sup>33</sup>M. Brahlek, L. Zhang, C. Eaton, H.-T. Zhang, and R. Engel-Herbert, *Appl. Phys. Lett.* **107**, 143108 (2015).
- <sup>34</sup>M. Mirjolet, F. Sánchez, and J. Fontcuberta, *Adv. Funct. Mater.* **29**, 1808432 (2019).
- <sup>35</sup>M.S.J. Marshall, D.T. Newell, D.J. Payne, R.G. Egdell, and M.R. Castell, *Phys. Rev. B* **83**, 035410 (2011).
- <sup>36</sup>Y. Bourlier, M. Frégnaux, B. Bérini, A. Fouchet, Y. Dumont, and D. Aureau, *ChemNanoMat* **5**, 674 (2019).
- <sup>37</sup>C. Lin, A. Posadas, T. Hadamek, and A.A. Demkov, *Phys. Rev. B* **92**, 035110 (2015).

- <sup>38</sup>Y. Bourlier, M. Frégnaux, B. Bérini, A. Fouchet, Y. Dumont, and D. Aureau, *Appl. Surf. Sci.* **553**, 149536 (2021).
- <sup>39</sup> See supplementary material at [URL will be inserted by AIP Publishing] for IMFP calculations and full XPS and XRD data.
- <sup>40</sup>C. J. Powell, *J. Vac. Sci. Technol. A.* **38**, 023209 (2020).
- <sup>41</sup>A.B. Posadas, K.J. Kormondy, W. Guo, P. Ponath, J. Geler-Kremer, T. Hadamek, and A.A. Demkov, *J. Appl. Phys.* **121**, 105302 (2017).
- <sup>42</sup>P.S. Bagus, E. Ilton, and C.J. Nelin, *Catal. Letters* **148**, 1785 (2018).
- <sup>43</sup>R. Eguchi, M. Taguchi, M. Matsunami, K. Horiba, K. Yamamoto, A. Chainani, Y. Takata, M. Yabashi, D. Miwa, Y. Nishino, K. Tamasaku, T. Ishikawa, Y. Senba, H. Ohashi, I.H. Inoue, Y. Muraoka, Z. Hiroi, and S. Shin, *J. Electron Spectros. Relat. Phenomena* **156–158**, 421 (2007).
- <sup>44</sup>J. Laverock, J. Kuyyalil, B. Chen, R.P. Singh, B. Karlin, J.C. Woicik, G. Balakrishnan, and K.E. Smith, *Phys. Rev. B* **91**, 165123 (2015).
- <sup>45</sup>T. Katayama, A. Chikamatsu, K. Yamada, K. Shigematsu, T. Onozuka, M. Minohara, H. Kumigashira, E. Ikenaga, and T. Hasegawa, *J. Appl. Phys.* **120**, 085305 (2016).
- <sup>46</sup>B. Koo, K. Kim, J.K. Kim, H. Kwon, J.W. Han, and W. Jung, *Joule* **2**, 1476 (2018).
- <sup>47</sup>K. Szot, W. Speier, U. Breuer, R. Meyer, J. Szade, and R. Waser, *Surf. Sci.* **460**, 112 (2000).
- <sup>48</sup>R. Meyer, R. Waser, J. Helmbold, and G. Borchardt, *J. Electroceramics* **9**, 101 (2002).
- <sup>49</sup>W. Jung and H.L. Tuller, *Energy Environ. Sci.* **5**, 5370 (2012).
- <sup>50</sup>M. Andrä, H. Bluhm, R. Dittmann, C.M. Schneider, R. Waser, D.N. Mueller, and F. Gunkel, *Phys. Rev. Mater.* **3**, 044604 (2019).
- <sup>51</sup>S.N. Ruddlesden and P. Popper, *Acta Crystallogr.* **11**, 54 (1958).
- <sup>52</sup>S. Šturm, A. Rečnik, C. Scheu, and M. Čeh, *J. Mater. Res.* **15**, 2131 (2000).

This is the author's peer reviewed, accepted manuscript. However, the online version of record will be different from this version once it has been copyedited and typeset.  
PLEASE CITE THIS ARTICLE AS DOI: 10.1116/6.0001419

- <sup>53</sup>B. Bérini, V. Demange, M. Bouttemy, E. Popova, N. Keller, Y. Dumont, and A. Fouchet, *Adv. Mater. Interfaces* **3**, 1600274 (2016).
- <sup>54</sup>R.C. Germanicus, Y. Bourlier, V. Notot, B. Bérini, V. Demange, M. Berthe, A. Boileau, M. Euchin, Y. Dumont, D. Aureau, M. Fregnaux, B. Grandidier, U. Lüders, A. David, W. Prellier, L. Biadala, and A. Fouchet, *Appl. Surf. Sci.* **510**, 145522 (2020).
- <sup>55</sup>E. Mutoro, E.J. Crumlin, M.D. Biegalski, H.M. Christen, and Y. Shao-Horn, *Energy Environ. Sci.* **4**, 3689 (2011).
- <sup>56</sup>Y. Yu, H. Luo, D. Cetin, X. Lin, K. Ludwig, U. Pal, S. Gopalan, and S. Basu, *Appl. Surf. Sci.* **323**, 71 (2014).
- <sup>57</sup>F.V.E. Hensling, C. Baeumer, M.-A. Rose, F. Gunkel, and R. Dittmann, *Mater. Res. Lett.* **8**, 31 (2020).

## Tables

TABLE I. Binding energy (BE), percentage of total area (% Area), full width at half maximum (FWHM) and doublet separation of the different components used to fit the V  $2p_{3/2}$  and Sr  $3d_{5/2}$  XPS spectra for bare and capped SVO samples.

	Bare SVO				Capped SVO			
	BE (eV)	%Area	FWHM (eV)	Doublet separation (eV)	BE (eV)	%Area	FWHM (eV)	Doublet separation (eV)
V $2p_{3/2}$ ( $V^{4+}$ )	515.08	8.4	2.38	7.28	515.03	100	3.65	
V $2p_{3/2}$ ( $V^{5+}$ )	517.07	91.6	1.64	7.51				
Sr $3d_{5/2}$ (SVO)	132.04	5.1	0.80	1.80	132.00	44.7	1.04	1.78
Sr $3d_{5/2}$ (Surface)	133.35	94.9	1.81	1.77	133.30	55.3	1.64	1.75



## Figure captions

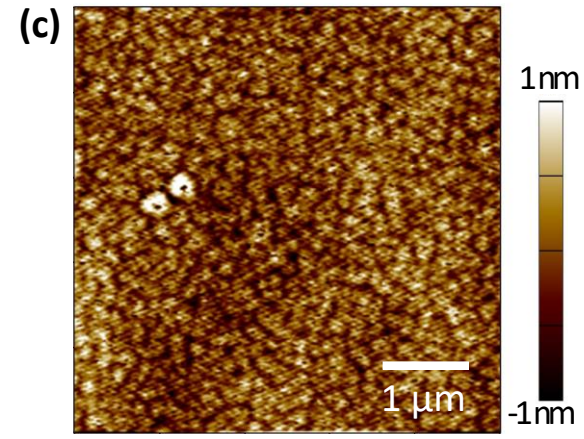
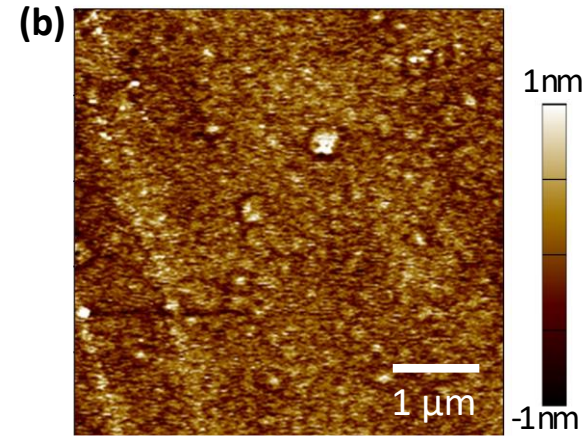
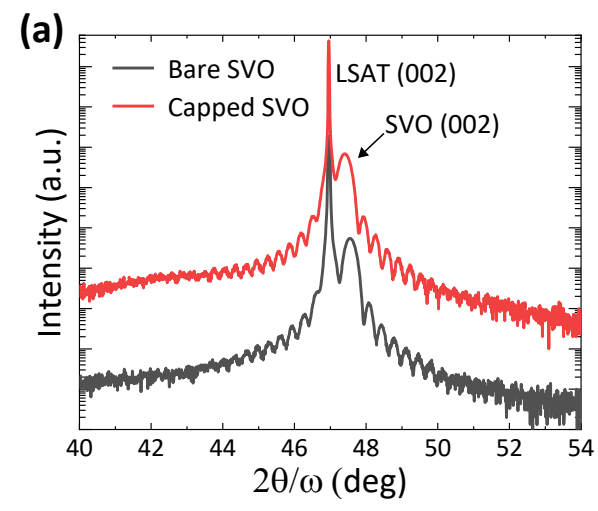
FIG. 1. (a) X-ray diffraction patterns around the (002) Bragg reflection of bare (black) and capped (red) SVO films, grown on LSAT substrates. Representative AFM image of (b) bare and (c) capped SVO films, acquired from an area of  $5 \times 5 \mu\text{m}^2$ .

FIG. 2. High resolution XPS spectrum of Ti  $2p_{3/2}$  core level of the capped SVO sample.

FIG. 3. (a) Background-subtracted XPS spectra of O 1s and V 2p core levels of bare SVO and capped SVO. The inset shows schematic structures of both samples. (b) Fit of the V  $2p_{3/2}$  spectral region of bare SVO and capped SVO (inset). The fitted curve of the capped SVO is also presented, magnified and vertically shifted, under the bare SVO signal, for comparison.

FIG. 4. Background-subtracted XPS spectra and fit of Sr 3d core level for bare SVO (bottom) and capped SVO (top, magnified and vertically shifted for clarity).

This is the author's peer reviewed, accepted manuscript. However, the online version of record will be different from this version once it has been copyedited and typeset.  
PLEASE CITE THIS ARTICLE AS DOI: 10.1116/6.0001419



This is the author's peer reviewed, accepted manuscript. However, the online version of record will be different from this version once it has been copyedited and typeset.  
PLEASE CITE THIS ARTICLE AS DOI: 10.1116/6.0001419

